Pergamon

Geochimica et Cosmochimica Acta, Vol. 68, No. 6, pp. 1185–1197, 2004

0016-7037/04 $30.00 + .00

doi:10.1016/j.gca.2003.07.015

Formation and stability of schwertmannite in acidic mining lakes

SIMONA REGENSPURG,[1,*] ANDREAS BRAND,[2] and STEFAN PEIFFER[3]

[1]Institute for Chemistry and Geochemistry, Colorado School of Mines, Golden, CO 80401, USA
[2]Institute of Applied Mathematics, University of Erlangen-Nürnberg, Martensstr. 3, D-91058 Erlangen, Germany
[3]Institute for Hydrogeology, RWTH Aachen, Lochnerstr. 4-20, D-52064 Aachen, Germany

(*Received September* 4, 2002; *accepted in revised form July* 9, 2003)

Abstract—Schwertmannite (ideal formula: $Fe_8O_8(OH)_6SO_4$) is typically found as a secondary iron mineral in pyrite oxidizing environments. In this study, geochemical constraints upon its formation are established and its role in the geochemical cycling of iron between reducing and oxidizing conditions are discussed. The composition of surface waters was analyzed and sediments characterized by X-ray diffraction, FTIR spectroscopy and determination of the Fe:S ratio in the oxalate extractable fraction from 18 acidic mining lakes. The lakes are exposed to a permanent supply of pyritegenous ferrous iron from adjacent ground water. In 3 of the lakes the suspended matter was fractionated using ultra filtration and analyzed with respect to their mineral composition. In addition, stability experiments with synthetic schwertmannite were performed. The examined lake surface waters were O_2-saturated and have sulfate concentrations (10.3 ± 5.5 mM) and pH values (3.0 ± 0.6) that are characteristic for the stability window of schwertmannite. Geochemical modeling implied that i) the waters were saturated with respect to schwertmannite, which controlled the activity of Fe^{3+} and sulfate, and ii) a redox equilibrium exists between Fe^{2+} and schwertmannite. In the uppermost sediment layers (1 to 5 cm depth), schwertmannite was detectable in 16 lakes—in 5 of them by all three methods. FTIR spectroscopy also proved its occurrence in the colloidal fraction (1–10 kDa) in all of the 3 investigated lake surface waters. The stability of synthetic schwertmannite was examined as a function of pH (2–7) by a 1-yr experiment. The transformation rate into goethite increased with increasing pH. Our study suggests that schwertmannite is the first mineral formed after oxidation and hydrolysis of a slightly acidic (pH 5–6), Fe(II)-SO_4 solution, a process that directly affects the pH of the receiving water. Its occurrence is transient and restricted to environments, such as acidic mining lakes, where the coordination chemistry of Fe^{3+} is controlled by the competition between sulfate and hydroxy ions (i.e. mildly acidic).

1. INTRODUCTION

Schwertmannite is an iron(III) oxyhydroxysulfate with the general formula $Fe_8O_8(OH)_xSO_y \cdot n\ H_2O$ where $8 - x = y$ and $1.0 \leq y \leq 1.75$ and a mineral structure akin to that of akaganéite (β-FeOOH), which is metastable with respect to goethite (α-FeOOH) (Bigham et al., 1990, 1996). Since its first description as a pure mineral phase (Bigham et al., 1990), schwertmannite had been found in a number of environments, mainly affected by acid mine drainage (AMD) (Bigham et al., 1994, Yu et al., 1999) but also under undisturbed conditions (Childs et al., 1998, Schwertmann et al., 1995). It typically forms in acidic, sulfate-rich waters draining through iron sulfide containing rocks and soils (Bigham et al., 1990; Schwertmann et al., 1995).

Due to its poor crystallinity, variable composition and similarity to other minerals such as akaganéite, jarosite and goethite (Bigham et al., 1990, 1996), schwertmannite may be difficult to structurally identify and little information exists about the geochemical requirements for its formation and stability. In acidic sulfate solutions, the favorable pH of schwertmannite occurrence ranges between 2.5 and 4.5, while jarosite dominates at pH < 2.5 (Cravotta et al., 1999). Schwertmannite formation seems to be directly linked to the bacterially catalyzed oxidation of Fe^{2+} (Kawano and Tomita, 2001). Recently, its role in the electron cycling in the sediment of an acidic lignite mining lake (AML) had been stressed (Peine et al., 2000), where schwertmannite serves as an electron acceptor for Fe(III) reducing bacteria (Küsel et al., 1999). Its transformation to goethite releases acidity, a process which seems to inhibit sulfate reduction in these sediments and to support an acidic iron cycle at the sediment-water interface (Peine et al., 2000). Schwertmannite can therefore be regarded to be a key intermediate in the transition process from iron reducing to iron oxidizing conditions.

It appears that hydrochemical conditions in AML, which cover a narrow pH range between 2 and 4 and receive anoxic, Fe(II)- and sulfate-rich ground water (Geller et al., 1998), are favorable for the formation of schwertmannite. High sedimentation rates of schwertmannite have been observed in ML 77, which had been directly linked to the oxidation of Fe^{2+} in the lake water (Peine et al., 2000). These lakes can be looked at as model systems that allow direct insight into the geochemical processes responsible for the occurrence of schwertmannite. In particular they allow the study of the following key questions: i) to what extent is the formation of schwertmannite linked to the oxidation of Fe(II), is it affected by the high concentrations of sulfate, and how are these processes related to the pH of the lake waters, and ii) what affects the stability of schwertmannite with respect to transformation into either goethite or jarosite?

In a broader sense, this study aims to elucidate the role of this mineral for the chemical composition of the lakes′ waters and for the geochemical processes within the lakes. We therefore examined the chemical composition of surface lake water and sediments from 18 lakes located in different mining areas as

* Author to whom correspondence should be addressed (simona_purg@web.de).

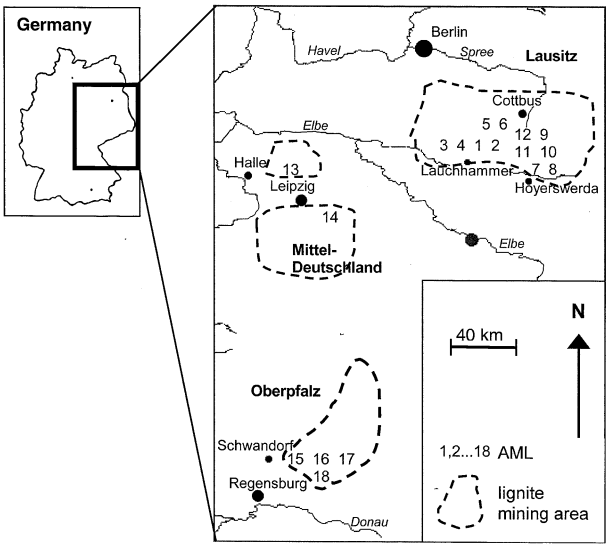

Fig. 1. Location of the 18 investigated AML in three mining areas in Germany: Oberpfalz, Mitteldeutschland and Lausitz.

Table 1. Site description of the 18 AML investigated (Peine, 1998; LMBV, 1997: this study).

No.	Lake name	Region	Lake age[a]	Surface (ha)	Volume (m^3) or depth (m)
1	ML 77	Lausitz	~40	24	max. depth: 7 m
2	ML 117		~40	~60	max. depth: 13 m
3	ML 107		~40	—	—[b]
4	ML 111		~40	~100	—[b]
5	ML 13		~3[c]	38	5 Mio
6	ML F		3[c]	234	25 Mio
7	Spreetal NO		4[c]	314	97 Mio
8	Kortitzmühle		~30	—[c]	—
9	Koschen		3	620	39 Mio
10	Bluno		3[c]	1211	152 Mio
11	Skado		3[c]	980	130 Mio
12	Sedlitz		3[c]	1311	141 Mio
14	Borna Ost	MittelDeutschland	2[c]	—[b]	—[b]
13	Niemegk		3	—[b]	—[b]
15	Murnersee	Oberpfalz	23	145	max. depth: 45 m
16	Brückelsee		22	24	max. depth: 40 m
17	Ausee		20	90	max. depth: 30 m
18	Lindensee		20	121	max. depth: 12 m

[a] Years since flooding began.
[b] Data were not available.
[c] Flooding not yet finished.

well as the colloidal matter from 3 of these lakes. Additionally, we synthesized schwertmannite in the laboratory and measured its stability as a function of time and pH.

2. MATERIALS AND METHODS

2.1. Study Sites

The 18 investigated AML are located in three different lignite mining areas in Germany: Lausitz, Mitteldeutschland and Oberpfalz (Fig. 1). The lignite formed during the Tertiary (Miocene) in a freshwater environment (Landesumweltamt Brandenburg, 1995). In the Lausitz mining area, the Tertiary sediments are covered by Quaternary glacial sediments, mostly sands and till marls (Nowel et al., 1995). Iron sulfide (mainly marcasite) content in the lignite can reach up to 3 wt% and in the lignite containing dumps it ranges between 0.002 and 1.05 wt% (Landesumweltamt Brandenburg, 1995). Tertiary and Cretaceous sediments of sand and clay form sediments of the mining area in the Oberpfalz (Meyer and Mielke, 1993). Lignite, embedded in highly permeable Miocene sands, contained 1.8 to 2.6 wt% pyrite (Meyer and Poschlod, 1993). In the Mitteldeutschland mining area, the dumps contain up to 4% pyrite. Further minerals are mostly quartz 50–90%, feldspar (5–20%) and kaolinite (0–10%) (Krüger et al., 1998).

All investigated lakes are affected by ground water passing through dump material and are therefore influenced by AMD. Table 1 gives an overview of names, location and morphometric data of the lakes.

2.2. Sampling

Sampling of sediment and lake water was carried out between August and October 2000, during the stagnation period of the lakes. In ML 77 samples were taken in summer 1997 (Peine, 1998).

Depth profiles of pH, oxygen, temperature and electrical conductivity were measured with a multi-parameter probe in the surface waters. Water samples were taken 1 m below the surface. The samples were filtered (0.2 μm) in the field, cooled during transport and stored deep-frozen in the laboratory before further investigation. A subsample of 100 mL was acidified with 0.1 mL concentrated HNO_3 (65%) in the field and the Fe^{2+} concentration was determined photometrically the same day in the laboratory.

Sediment cores were taken with a gravity corer (∅ 6 cm; 50 cm length) in Plexiglas tubes from the deepest part or from the centre of the lakes. Immediately after arrival in the laboratory, the upper 1- 5 cm orange to yellow layers of the cores, which could be distinguished visually from the deeper, dark-brown or grey colored layers, were separated, flushed with N_2 and deep-frozen. Before further analysis the samples were defrosted, filtered (blue-ribbon, Schleicher and Schüll) and freeze-dried.

Water samples for the study of suspended material were taken 1 m above ground from three mining lakes (ML 77, ML117 and Borna Ost) in April 2001. The samples were cooled during transport and stored for 2 d in a dark room at 4°C before further processing in the laboratory.

2.3. Analytical Methods

pe values of the lake waters were determined using a platinum cell calibrated against chinhydron saturated pH buffer solutions. SO_4^{2-}, Cl^-, Ca^{2+}, Mg^{2+}, K^+, Na^+ and NH_4^+ were measured by ion chromatography, Fe(II) photometrically by the phenanthroline method (Tamura et al., 1974), Fe(tot) and Al-(tot) by flame AAS. Fe(III) was taken as the difference between Fe(tot) and Fe(II).

Due to the uncertainty inherent to the determination of weakly crystalline iron minerals, three independent methods were applied to identify the mineral composition of the sediments.

(1) Samples (0.05 g) were extracted with 0.05 L acid am-

Table 2. Determination of the solubility-product and the Fe(III) activity of schwertmannite (Sh), ferrihydrite (Fh), K-jarosite (Jt), and goethite (Gt).

Mineral	Dissolution reaction	Log K	Eqn.
Sh	$Fe_8O_8(OH)_x(SO_4)_y + (24 - 2y)H^+ \Rightarrow 8\ Fe^{3+} + y\ SO_4^{2-} + (24 - 2y + x)/2H_2O$	18 ± 2.5[a]	(1)
Fh	$Fe(OH)_3 + 3H^+ \Rightarrow Fe^{3+} + 3\ H_2O$	4.81[b]	(2)
Jt	$KFe_3(SO_4)_2(OH)_6 + 6H^+ \Rightarrow 3\ Fe^{3+} + 6\ H_2O + K^+ + 2\ SO_4^{2-}$	−9.21[b]	(3)
Gt	$FeOOH + 3H^+ \Rightarrow Fe^{3+} + 2H_2O$	1.4[a]	(4)

[a] Bigham et al. (1996).
[b] Parkhurst (1995).

monium oxalate (pH 3) for 15 min in the absence of light (Carlson and Schwertmann, 1981; Bigham et al., 1990) to separate schwertmannite (dissolves completely) from insoluble goethite and jarosite. In the extracts Fe and Al were determined by flame-AAS and S by ICP-AES. To receive the total concentration of Al, Fe and S contained in the sediments, these elements were additionally measured in samples extracted with 6 mol/L HCl, heated at 70°C for 30 min. In separate experiments it was shown that synthetic goethite and jarosite dissolve completely by this procedure.

(2) The minerals were identified by powder X-ray diffraction (XRD) using a Siemens D 5000 X-ray diffractometer with Co-K$\alpha_{1,2}$-radiation (40 kV; 40 mA) after grinding the samples. Counting rate was either 2 s/0.02° 2 θ or 8 s/0.01° 2 θ. Minerals were identified either with the library evaluation-program DiffracAT Vers. 3.3 or, in the case of schwertmannite, by comparison with a schwertmannite standard, synthesized in our laboratory (the diffraction pattern was identical to that of schwertmannite described by Bigham et al., 1990).

(3) Transmission FTIR spectra of KBr pelleted samples with 1 cm^{-1} resolution were generated with a Vektor 22 Bruker FTIR spectrometer. 32 scans were collected for each measurement. Pellets were produced as homogenous mixture of 3 mg sample and 300 mg KBr pressed with a hydraulic press at a load of ~8 tons. The absorption intensities were determined as the maximum height over baseline. They were identified with the evaluation program OPUS-NT and compared to mineral libraries of Farmer (1974), Van der Marel and Beutelspacher (1976) and the IR spectrum of schwertmannite described by Bigham et al. (1990). To eliminate interference from kaolinite or other silicates the spectra of the oxalate insoluble fraction were subtracted from those of the original sample.

Scanning electron microscopy (SEM) was performed with a Leo 1530 with a ZrO_2 radiation source on tungsten- wire. Samples were covered with platinum layer before measurement. The specific surface area was determined by a five point N_2 gas adsorption isotherm (BET) method. Just before measurement, samples were heated at 110°C (30 min) in glass tubes (to eliminate completely any moisture) and then weighed.

Procedures of drying, pressing or heating samples did not result in structurally changes of the solid samples as demonstrated by XRD with synthetic minerals in separate experiments.

2.4. Treatment of Suspended Matter (Colloidal Material)

Suspended particles from three mining lakes (ML 77, ML117 and Borna Ost) were collected by first prefiltering of 1 L surface water through a 0.2 μm cellulose acetate filter. Subsequently particles were removed from the filters after 15 min ultrasound treatment in ultra pure water (10 mL), enriched by 20 min centrifugation at 20800 rpm and dried at 60°C. The filtrate was fractionated by ultra filtration using different cellulose membranes (Amicon ultrafiltration system) at 1, 10 and 100 kDa (1 kDa ~ 1 nm; 100 kDa ~ 10 nm pore size) and at a N_2-overpressure of 3.5 bar in two steps. First, 50 mL of the sample were pressed through each of the filters. Iron was determined in all, and sulfate in two of the ultrafiltrates, in four replicates. In a second step, the remaining 800 mL of the sample were successively pressed through the three membranes. The filter residues of the fractions were enriched by centrifugation (3 times for 20 min and 20,800 rpm) and finally dried (60°C) and analyzed by FTIR.

2.5. Geochemical Modeling

The geochemical computer code PhreeqC (version 2.2; Parkhurst and Appelo, 1999) was used to calculate chemical equilibria between the solid and dissolved phase in the lakes and to predict the dominating species and ionic complexes in the water as well as the formation of minerals. Most stability constants were taken from the PhreeqC data file, which is based on the compilation by Nordstrom et al. (1990). Eqns. 1 to 4 in Table 2 provide the solubility functions of the four Fe minerals considered in this study, i.e., goethite, jarosite, schwertmannite and ferrihydrite according to Bigham et al. (1996) and Parkhurst (1995). The program calculates ionic activities using the Davies equation and charge imbalances (Eqn. 5).

$$L = \frac{\sum_{i}^{N^-} c_i^-|z_i| - \sum_{j}^{N^+} c_j^+|z_j|}{\sum_{i}^{N^-} c_i^-|z_i| + \sum_{j}^{N^+} c_j^+|z_j|} \cdot 100 \qquad (5)$$

where L = charge imbalance (%),

n_j^+, n_i^-, c_j^+, c_i^- = concentration of positively (j)/negatively (i) charged species i and j(M),

z_i, z_j = charge of species i/j, and

N^+, N^- = number of the positively/negatively species

To determine the effect of the charge imbalance on the calculated activity, we calculated the relative error r for the activity of each species for a given charge imbalance (which was adjusted by variation of the sulfate concentration) using Eqn. 6.

Table 3. Chemical characteristics of AML surface waters (mean value for concentrations in mM), taken 1 m below surface, sampling time was mostly in summer 2000 or in summer 1997 (ML 77).[a]

ML	pH	pe	SO_4^{2-}	O_2	Fe(III)	Fe(II)	Al	Na	K	NH_4	Ca^{-}	Mg
ML 77[b]	2.9	n.m.	8.5	0.28	1.5	0.03	0.11	0.07	n.m.	n.m.	4.7	0.80
ML 107	2.3	13.8	6.5	n.m.	11.1	0.04	2.9	0.22	0.32	0.44	9.4	0.60
ML 117	3.0	13.4	9.3	0.30	0.3	0.004	0.07	0.39	0.14	0.12	2.5	0.58
ML 111	2.7	13.3	14.9	0.26	2.6	0.055	1.6	0.27	0.19	0.14	5.3	1.2
ML 13	2.9	12.8	7.5	0.29	0.23	0.028	0.27	0.26	0.17	0.05	2.5	0.23
ML F	2.8	12.9	17	n.m.	0.5	n.d.	n.d.	1.3	0.15	n.d.	2.4	0.55
Spreetal NO	3.6	10.8	10.4	0.24	0.01	0.001	0.17	1.0	0.38	n.d.	7.6	2.6
Kortitzmühle	4.7	7.8	12.4	0.27	0.004	n.d.	n.d.	0.96	0.29	0.21	13.6	2.2
Koschen	3.1	12.4	7.6	0.26	0.22	0.001	0.06	1.5	0.29	0.13	4.7	1.2
Bluno	2.9	13.2	13.7	0.27	0.9	0.015	0.24	0.79	0.32	0.11	5.0	1.7
Skado	2.8	13.4	18	0.28	1.5	0.017	0.30	0.87	0.28	0.22	7.0	2.1
Sedlitz	3.0	13.2	18.6	0.28	0.4	0.010	0.34	2.3	0.34	0.21	7.8	1.8
Borna Ost	2.9	13.7	19.4	0.27	1.2	0.021	7.9	0.42	0.11	n.d.	8.9	1.4
Niemegck	4.7	4.5	3.4	0.28	n.d.	n.d.	n.m.	1.3	0.15	n.d.	2.4	0.55
Murner See	3.3	13.3	3.2	0.25	0.025	0.028	0.22	0.24	0.11	n.d.	1.9	0.39
Brückelsee	3.1	n.m.	3.4	0.27	0.54	0.024	0.29	0.19	0.12	n.d.	3.9	0.36
Ausee	3.0	n.m.	4.6	0.25	0.183	0.033	0.37	0.39	0.14	0.04	1.4	0.35
Lindensee	2.8	n.m.	6.6	0.24	0.27	0.078	0.87	0.16	0.12	0.04	5.8	0.39

[a] n.d., not detected; n.m., not measured.
[b] Peine (1998).

$$r\,(\log a\,(i)) = \frac{|\log a_L(i)| - |\log a_0(i)|}{|\log a_0\,(i)|} \qquad (6)$$

where $\log a_L\,(i)$ = logarithm of the activity of species i at change imbalance L and $\log a_0\,(i)$ = logarithm of the activity of species i at $L = 0$.

2.6. Synthetic Samples

Schwertmannite was synthesized by two different procedures: method 1 (long-term synthesis) takes approximately 30 d and was described by Bigham et al. (1990): 2 L of deionized water were heated in an oven to 60°C. After adding 10.8 g $FeCl_3 \cdot 6H_2O$ ($\sim$ 40 mM Fe^{3+}) and 3 g Na_2SO_4 ($\sim$ 10 mM SO_4^{2-}) the solution was kept for further 12 min at 60°C. The orange colored suspension was dialyzed in cellulose membranes (Serva dialysis bags, pore radius of 2.4 nm) against deionized water ($\sim$ 4 L), which was renewed on a daily basis over a period of 33 d. When the electric conductivity in the water remained $< 5\ \mu S \cdot cm^{-1}$, the precipitate was filtered and freeze-dried. This procedure yields approx. 2 g schwertmannite, identified by XRD. Based on the Fe and S content in a HCl-extract (c = 1 mol/L), an average stoichiometry of $Fe_8O_8(OH)_{5.5}(SO_4)_{1.3}$ was determined.

Method 2 follows a recipe kindly provided by H.J. Pentinghaus (private communication). 10 g $FeSO_4$ are dissolved in 1 L distilled water and reacted with 5 mL H_2O_2 (32%). The solution becomes dark-red and a red-orange material precipitated. After $\sim$24 h the pH in the solution remained stable (2.4) and the solid was filtered and freeze-dried. Fe and sulfate determination of the XRD-identified schwertmannite confirmed an average chemical formula of $Fe_8O_8(OH)_{3.9}(SO_4)_{2.1}$.

Goethite was produced by reaction of $Fe(NO_3)_3$ with KOH according to the recipe described by Cornell and Schwertmann (1996).

2.7. Stability Experiment

Synthetic schwertmannite, synthesized by method (1) was transferred as suspension directly from the dialysis bags into five different glass vessels. Each vessel contained $0.75\ g \cdot L^{-1}$ schwertmannite. The pH in the vessels was adjusted to 2, 3, 4, 5, and 7 by adding HNO_3 or NaOH. The pH was measured and adjusted, if necessary, daily in all suspensions. The vessels were continuously stirred (electrically shaken) in a dark room at 25°C ± 1°C. From time to time aliquots were sampled and filtered through a blue ribbon filter. Sulfate and iron were measured in the filtrate and the solids were analyzed after drying (60°C) by FTIR spectroscopy. At the end of the experiment (after 362 d) the remaining solids were X-rayed.

3. RESULTS

3.1. Hydrochemistry of AML

As shown in Table 3, surface waters of all AML had low pH values (2.3 to 4.7) and high sulfate concentrations (3 to 19 mM). The predominant cations were calcium (1.4 to 13.6 mM), magnesium (0.2 to 2.6 mM), aluminium (0.06 to 7.9 mM) and iron (0 to 11 mM), both in the ferric and ferrous form. Fe(III) concentrations generally exceeded that of Fe(II) and the O_2 concentration was between 0.24 and 0.3 mM.

Calculation of the chemical speciation indicated that in all lakes with pH values < 3.5, Fe(III) was predominantly ($\sim$75% of total Fe(III)) complexed with sulfate ($Fe(SO_4)^+$ and $Fe(SO_4)_2^-$), the remaining species mainly consisting of hydroxy complexes and to a little extent of Fe^{3+}. Approximately 50% of dissolved Fe(II) was Fe^{2+}, $\sim$30% $FeSO_4$ and $\sim$20% $FeHSO_4^+$. Table 4 gives an example of the calculated Fe(III) and sulfate species (log a) in five AML.

Figure 2 shows a plot of calculated activities of Fe^{3+} (all Fe(III)-species) as a function of pH and compares them with

Table 4. Highest concentrated iron and sulfate species calculated by PhreeqC for surface waters of some AML.

AML	log $a(Fe^{3+})$	log $a(Fe(OH)^{2+})$	log $a(Fe(OH)_2)^{+}$	log $a(Fe(OH)_3$	log $a(Fe(SO_4)^{+})$	log $a(Fe(SO_4)_2^{-})$	log $a(SO_4^{2-})$
Bluno	−4.95	−4.45	−5.18	−9.34	−3.26	−4.23	−2.29
Skado	−4.76	−4.36	−5.20	−9.46	−3.00	−3.88	−2.21
Borna Ost	−4.88	−4.39	−5.12	−9.28	−3.12	−3.99	−2.20
ML 117	−5.24	−4.79	−5.50	−9.66	−3.68	−4.72	−2.35
Murnersee	−6.22	−5.23	−5.50	−9.18	−4.99	−6.43	−2.77

the solubility functions of goethite, jarosite, 2-line ferrihydrite and schwertmannite (Table 2). For schwertmannite and jarosite a solubility range is provided reflecting their variable SO_4^{2-}- and K^+-content. For schwertmannite log $a(SO_4^{2-})$ varies between −1 and −1.5 (Bigham et al., 1996) and for jarosite between −1.85 and −2.5 and log a K^+ between −3.5 and −4.07 (Parkhurst, 1995). Nearly all samples are located in the solubility window of schwertmannite indicating that schwertmannite most likely controls the solubility of Fe^{3+} in most of the lakes. Saturation indices (SI) were positive for goethite and jarosite in 17 of the lakes and indicated equilibrium between the lake water and schwertmannite in 15 of the lakes.

Charge imbalances (Eqn. 5) can affect the relative error r for SO_4^{2-}- and Fe^{3+} activities (Eqn. 6). They were negative (between −10 and −30%) for most AML and in one lake −50% (ML 107) was found. The maximum error (r) due to this highest charge imbalance would result in an overestimate of the sulfate activity of 14% and in an underestimate of 11% for the Fe^{3+} activity relative to the activity determined by calculations of PhreeqC. Thus, the error of the calculated sulfate activity is lower than the assumed overestimation by the sulfate measurement.

3.2. Geochemical and Mineralogical Composition of the Upper Sediment Layers and of Suspended Matter

In Figure 3 B, the XRD patterns of two sediment samples ("Skado" and "Murnersee") are compared to the patterns of synthetic schwertmannite produced by both synthesis methods (Fig. 3A). The broad peaks of schwertmannite are visible in Skado, whereas they are missing in Murnersee. The distinct peaks in the natural samples correspond to quartz, kaolinite and goethite. XRD identified schwertmannite unambiguously in four and gives evidence for its occurrence in two lakes; jarosite was identified in two and goethite in five lakes (Table 5). Identification of schwertmannite in sediments of other lakes was not possible by XRD. Its presence however could not be ruled out due to the high background of more crystalline minerals (for example quartz and kaolinite). No other iron or

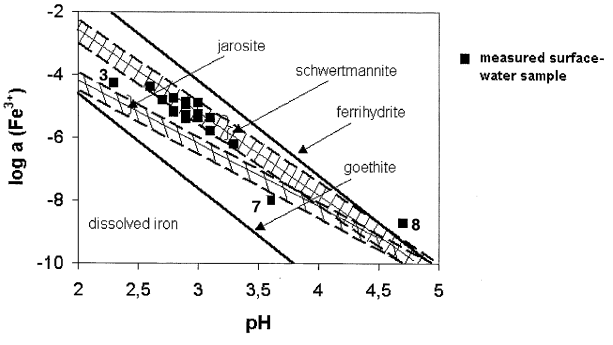

Fig. 2. Plot of the logarithm of the Fe^{3+} activity (mean values of measured data) versus pH for surface waters of 17 AML (Niemegk is not presented, because no iron was detected). Solubility lines were calculated (using the Eqns. 1 to 4 in Table 2) for goethite (log $a(Fe^{3+})$ = 1.4–3pH), ferrihydrite (log $a(Fe^{3+})$ = 4.83–3pH), K-jarosite (mid-line: log $a(Fe^{3+})$ = −0.19–2 pH) and schwertmannite (mid-line: log $a(Fe^{3+})$ = 2.7–2.63 pH). Maxima and minima (dashed lines) for the solubility window of schwertmannite are the range log $a(SO_4^{2-})$ = −1 to −1.5, that of jarosite −1.85 to −2.5 and for log $a(K^+)$ = −3.5 to −4.07. Presented numbers correspond to lakes (Table 1), situated outside the stability window of schwertmannite.

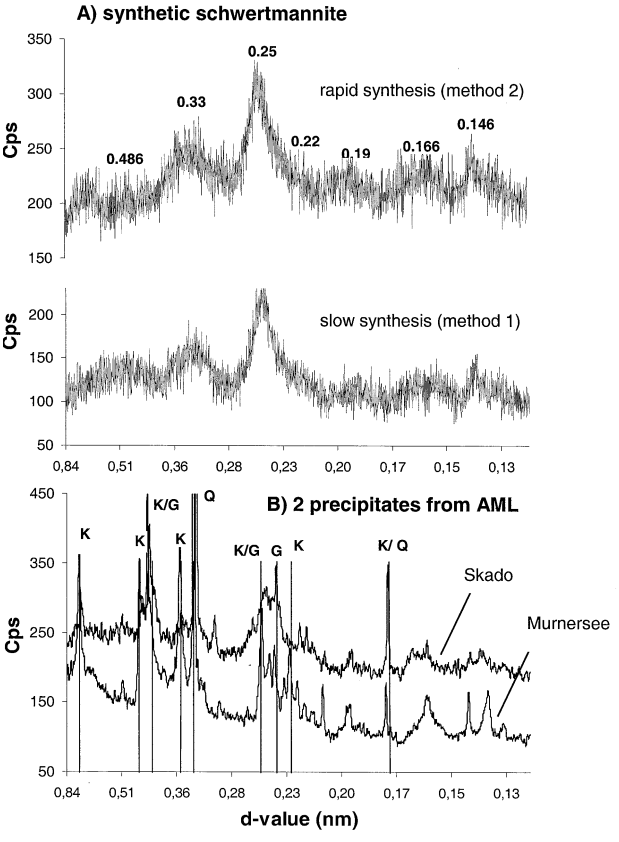

Fig. 3. X-ray diffraction pattern of synthetic (A) and natural samples (B). "Cps" are counts per second. A) Synthetic schwertmannite produced by two synthesis methods: numbers give d-values (nm) of schwertmannite peaks according to Bigham et al. (1990) B) Sediment samples from "Skado" and "Murnersee": the diffractogram of "Skado" shows some features of the schwertmannite (the large peak at 0.25 nm) and goethite (G) pattern, whereas the distinct peaks (marked by lines) in Murnersee are mainly dominated by kaolinite (K) and quartz (Q) peaks.

Table 5. Identification of iron minerals in the upper (1–5 cm) sediment layer of AML, based on XRD, Fe:S-ratios measured in the oxalate-extractable fraction and FTIR spectroscopy of sediment material and FTIR in the suspended matter. The column "estimated Fe-mineral inventory" summarizes the qualitative information obtained from all analytical methods.[a]

		Sediment			Suspended matter	
No.	AML	XRD	Fe/S	FTIR	FTIR	Estimated Fe-mineral inventory
1	ML 77	Sh	5.9 Sh	Sh	Sh	Sh
2	ML 107	(Sh), Gt	2.9 (Sh)	Sh, Gt	n.m.	(Sh), Gt
3	ML 117	(Sh), Jt, Gt	1.4 (Sh)	Sh, Jt	Sh	Sh, Jt
4	ML 111	Jt	2.6 (Sh)	Jt (Sh)	n.m.	Jt (Sh)
5	ML 13	i.n.p.	4.3 (Sh)	(Sh)	n.m.	(Sh)
6	ML F	i.n.p.	5.1 Sh	Sh	n.m.	(Sh)
7	Spreetal NO	i.n.p.	5.5 Sh	Sh	n.m.	(Sh)
8	Kortitzmühle	i.n.p.	16	Sh, Gt, Jt	n.m.	(Sh, Gt, Jt)
9	Koschen	Sh	4.7 Sh	Sh	n.m.	Sh
10	Bluno	i.n.p.	3.7 (Sh)	Sh, Jt	n.m.	(Sh, Jt)
11	Skado	Sh, Gt	4.9 Sh	Sh, Gt	n.m.	Sh, Gt
12	Sedlitz	Sh, Gt	5.1 Sh	Sh, Gt	n.m.	Sh, Gt
13	Borna Ost	i.n.p.	3.1 (Sh)	i.n.p.	Sh	Sh
14	Niemegck	Gt	7.9 Sh	Sh, Gt	n.m.	(Sh) Gt
15	Murner See	i.n.p.	1.3	i.n.p.	n.m.	i.n.p.
16	Brückelsee	i.n.p.	3.5 (Sh)	i.n.p.	n.m.	(Sh)
17	Ausee	i.n.p.	3.3 (Sh)	i.n.p.	n.m.	(Sh)
18	Lindensee	i.n.p.	1.5	i.n.p.	n.m.	i.n.p.

[a] Sh, schwertmannite; Gt, goethite; Jt, jarosite; i.n.p.; identification not possible with the methods used; n.m., not measured. Brackets indicate "probable."

sulfate minerals, such as ferrihydrite or gypsum, were identified by XRD.

In contrast to goethite and jarosite, schwertmannite and ferrihydrite are soluble in acid ammonium oxalate (Carlson and Schwertmann, 1981; Bigham et al., 1990). Therefore, the Fe:S ratio in the oxalate extract can be used as an indicator for the occurrence of schwertmannite. For schwertmannite it typically ranges between 5 and 8 and it is normally > 8 in the presence of ferrihydrite on which sulfate can only be adsorbed (Bigham et al., 1990). The oxalate extractable portion of the total sample exceeded 50% (dry-weight) in most of the sediment samples. Therein (Table 5), the Fe:S ratio indicated the occurrence of schwertmannite in seven lakes. Ratios lower than 5 were determined in ten lakes, in which schwertmannite may occur in addition to other soluble sulfate minerals not identified using XRD or FTIR. Due to low Al concentrations in the oxalate extracts (0–7 mg $\cdot$ g^{-1}) no competition with ferric iron (10–320 mg $\cdot$ g^{-1}) for sulfate was assumed. Significantly higher amounts of ferric iron in HCl extracts compared with oxalate extracts were found in ten lakes indicating the presence of another iron mineral (goethite or jarosite).

FTIR analysis shows that the sediment samples are composed of various phases as shown for "ML Skado," with bands of kaolinite and goethite (Fig. 4). However, its "difference spectrum," obtained after subtraction of the IR spectrum of the oxalate insoluble fraction from the sediment spectrum, is similar to the spectrum of synthetic schwertmannite (Fig. 4). Therefore, it can be assumed that the oxalate extractable fraction of the sediment consists of schwertmannite. By this method, schwertmannite was identified in the sediment of 11, goethite in 5 and jarosite in 4 lakes (Table 5).

Suspended matter was analyzed in three AML, each representing a different sediment composition (Table 5): in ML 77 it exclusively consists of schwertmannite, in ML 117 goethite, jarosite and schwertmannite occur and in the sediment layer of the relatively young lake Borna Ost (2 yr since flooding began, Table 1) no iron minerals could be identified probably due to the short time of iron sedimentation. Results of the filtrate analysis obtained from ultra filtration show that the colloidal bound iron and sulfate were mainly found in the fraction between 10 and 1 kDa (Table 6). FTIR spectroscopy identified the suspended material of the filter residue of each fraction to be schwertmannite in all three AML samples. An example (Borna Ost) of the fraction 1–10 kDa is presented in Figure 4. The FTIR spectra of samples obtained from the fraction > 0.22 μm (the residue of the prefiltration) show absorption bands of kaolinite only (e.g., Borna Ost in Fig. 4).

To summarize, schwertmannite unambiguously forms in six lakes, whereas its presence can be clearly excluded in only two lakes (Murnersee and Lindensee; Table 5). In the other lakes, identification using XRD failed or analysis of the composition of suspended matter was not performed. However, the other methods strongly indicate the occurrence of schwertmannite in 16 lakes altogether.

3.3. Synthetic Schwertmannite

Both synthetic schwertmannite specimens were, independent of the method by which they were produced, identical with respect to their XRD pattern (Fig. 3A) and have similar IR spectra (Fig. 4). They differ mostly in their surface characteristics: the specific surface area of the slowly synthesized schwertmannite (method 1) was much larger (175–220 m^2 $\cdot$ g^{-1}) compared to the specific surface area of rapidly crystallized (method 2) schwertmannite (4–14 m^2 $\cdot$ g^{-1}). Figure 5 shows scanning electron micrographs (SEM) of the synthesized and of a natural schwertmannite (ML 77). Particles (or crystal aggregates) formed by rapid synthesis are large spheroids with a

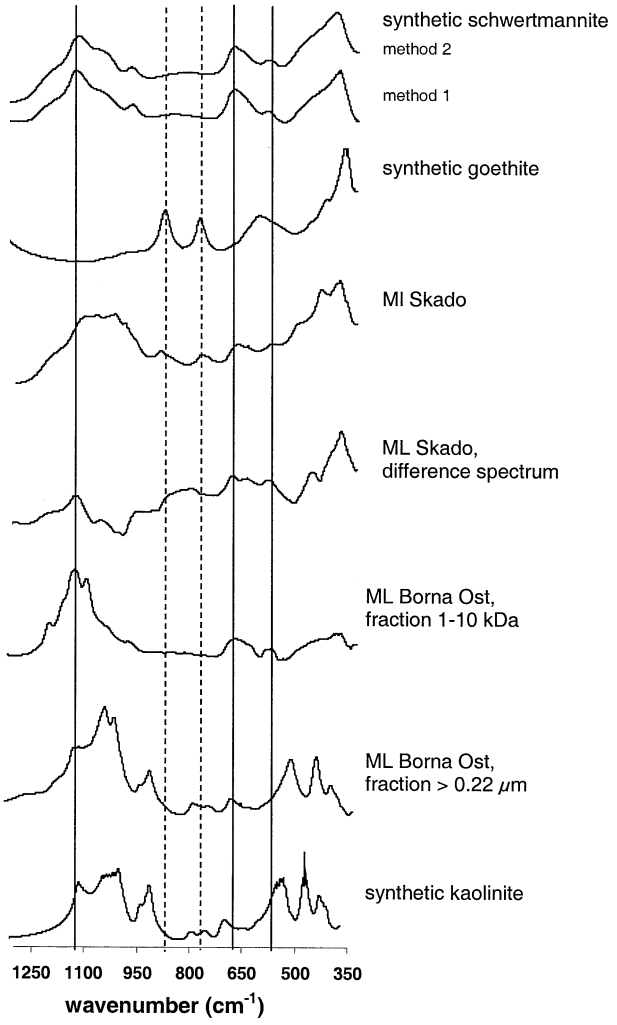

Fig. 4. FTIR-spectra of synthetic schwertmannite (produced by two synthesis methods), sediment sample "Skado", difference spectrum of "Skado" (difference between the signals of the untreated sample and that after NH_4-oxalate-extraction), the suspended matter of "Borna Ost" (fraction 1-10 kDa and > 0.22 μm) and synthetic kaolinite. Lines mark three significant absorption bands of schwertmannite (ν_3-SO_4 at 1124 cm^{-1}, ν-FeO at 704 cm^{-1} and ν_4 at 608 cm^{-1}) and dashed lines mark 2 bands of goethite (δ-OH at 892 cm^{-1} and γ-OH 797 cm^{-1}) according to Cornell & Schwertmann (1996).

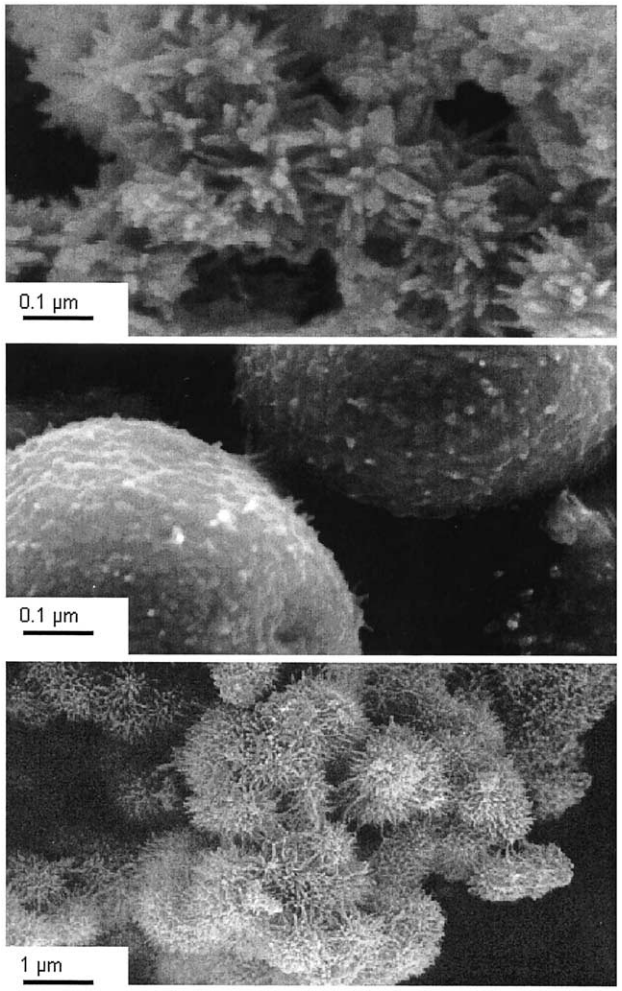

Fig. 5. Scanning electron micrographs (SEM) of schwertmannite samples: different morphologies can be observed after slow formation in dialysis bags (top), after rapid formation by oxidation of $FeSO_4$ with H_2O_2 (middle) and in a natural sample ("ML 77") (bottom).

diameter of $\sim$ 400 nm (Fig. 5). The slow synthesis method generated crystals, grown as long needles, which form the characteristic "hedge-hog" habit of schwertmannite particles. The natural sample had a specific surface area of 72 $m^2 \cdot g^{-1}$ and its morphology resembled that of the specimen synthesized by the long-time experiment.

3.4. Stability of Schwertmannite in Dependence of Time and pH

During the 1-yr stability experiment with synthetic schwertmannite as a function of pH, a release of sulfate occurred which was lowest at pH 3 (Fig. 6B). Sulfate release is initially linear,

Table 6. Characterisation of suspended matter: Iron and sulfate concentration (mM) in the filtrates of water samples obtained by ultra filtration.[a]

	<0.22 μm		<100 kDa		<10 kDa		<1 kDa	
	$Fe_{(tot)}$	SO_4^{2-}	$Fe_{(tot)}$	SO_4^{2-}	$Fe_{(tot)}$	SO_4^{2-}	$Fe_{(tot)}$	SO_4^{2-}
Borna Ost	1.188	18.76	1.211	n.m.	1.179	n.m.	1.004	18.309
ML 117	0.301	6.48	0.298	n.m.	0.299	n.m.	0.233	8.23
ML 77	1.915	14.31	1.918	n.m.	1.875	n.m.	1.298	9.973

[a] n.m., not measured.

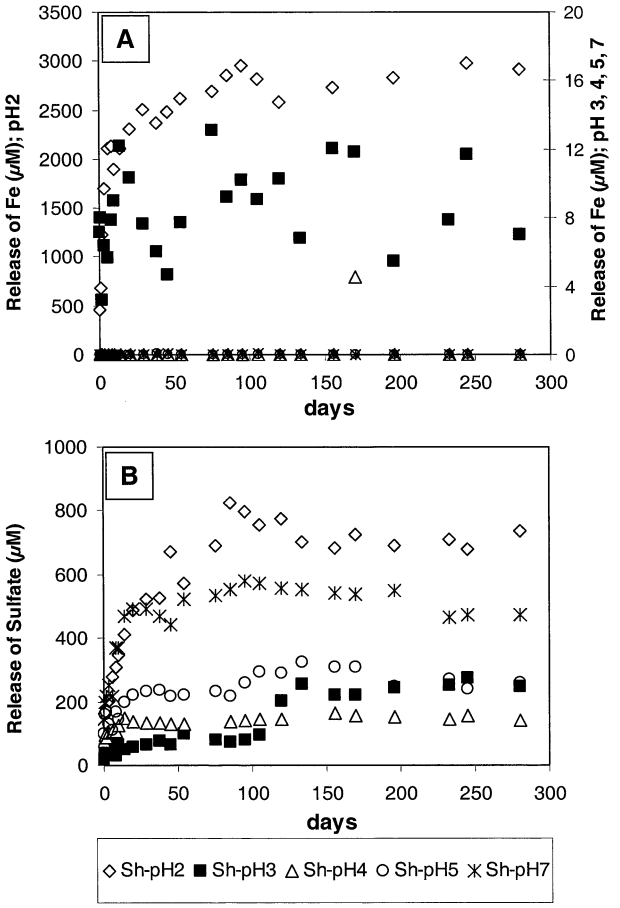

Fig. 6. Release of iron (A) and sulfate (B) in 5 schwertmannite suspensions (0.75 g L^{-1}) during 300 days at different pH (2, 3, 4, 5, 7). Note the two y-axis in Fig. 6A.

and after 30–100 d levels off to concentrations which correspond to 27% of total sulfate at pH 3, to 15% at pH 4, to 28% at pH 5 and to 49% at pH 7. The release rate was highest at pH 2 and an equilibrium was obtained after ~ 100 d with 70% of the total sulfate released. At pH 3 a second release could be observed after 100 d that doubled the amount of sulfate deliberated. The release rate of iron was significant at pH 2 only (~ 3000 μM which corresponds to 40% of total iron, Fig. 6A). It dropped to very low values at pH 3 (Fig. 6A, right y-axis) and was not detectable at higher pH-values.

XRD patterns of the solids kept at pH 2, 4 and 7, filtered in the end of the experiment, are shown in Figure 7. Goethite peaks (marked by lines) were identified in all diffractograms except in that of the sample kept at pH 2. At pH 2, the bulk of the solid dissolved during the experiment and the XRD pattern of the remaining material was marked by a very high background noise, indicating a weaker crystallinity (Fig. 7). The XRD patterns of the other samples demonstrate that with increasing pH, the intensity of the goethite peaks also increased. However, the broad peaks of schwertmannite were observed in all samples (Fig. 7). FTIR spectra recorded for the same samples show similar results with bands characteristic for both

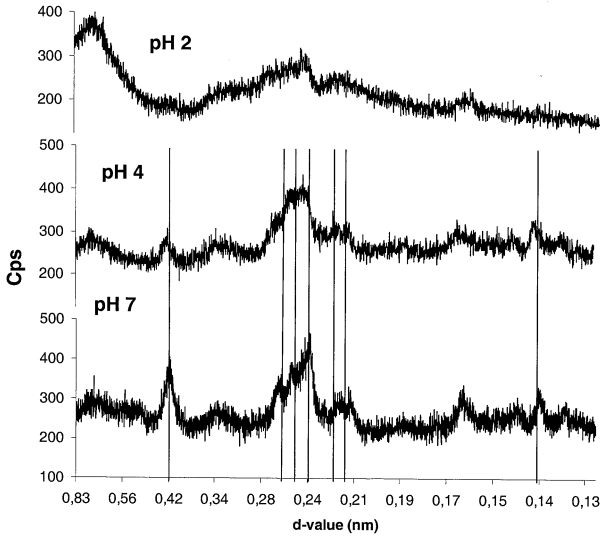

Fig. 7. X-ray diffraction patterns of solids kept at a constant pH-value of 2, 4 and 7 at the end (after 362 days) of the stability experiment. In the sample kept at pH 2, the highly intensive peak at 0.8 nm derives from the sample holder. The samples pH 4 and pH 7 show XRD-features of both schwertmannite and goethite. The goethite peaks dominate in the sample at pH 7 compared to the sample at pH 4. Lines mark some characteristic diffraction lines of goethite (Cornell & Schwertmann, 1996).

schwertmannite and goethite. The absorption intensities of the goethite bands increased with increasing pH (Fig. 8).

4. DISCUSSION

4.1. Occurrence of Schwertmannite in AML

Hydrochemistry of all examined lakes is characterized by high sulfate concentrations and the occurrence of both Fe(III) and Fe(II). The pH is fairly constant with only two of the lakes studied having a pH $>$ 4, and the mean value of the remaining 16 lakes of 3.0 $\pm$ 0.6 (Table 3). Such conditions are favorable to the formation schwertmannite which implies that this min-

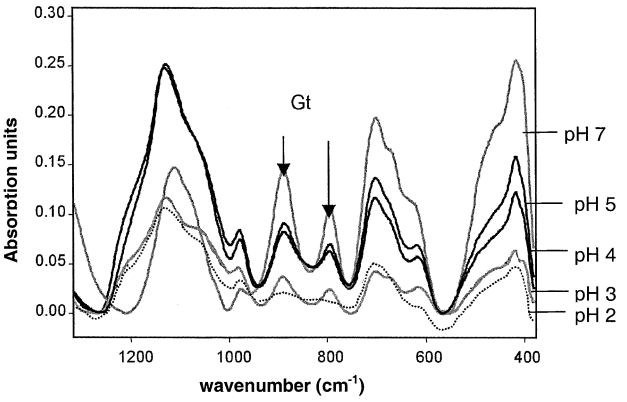

Fig. 8. FTIR spectra of solids kept at a constant pH-value of 2, 3, 4, 5 and 7 at the end (after 362 days) of the stability experiment. Bands marked with arrows indicate the formation of goethite, observed in nearly all samples. The intensity of this band decreases with decreasing pH.

eral should be a relevant solid Fe(III) phase in these environments. This hypothesis is based on three observations:

(1) A plot of the activity of Fe(III) versus pH (Fig. 2) shows that almost all lake water samples fall on a straight line, which reflects the solubility of schwertmannite and which indicates equilibrium between Fe(III) and schwertmannite. Most of the solutions are oversaturated with respect to the minerals jarosite and goethite.

(2) The colloidal matter in the investigated lakes is composed mainly of schwertmannite, which suggests schwertmannite to be the primary oxidation product of Fe(II) in the lake water. Neither goethite nor jarosite could be detected in this fraction.

(3) Schwertmannite appears to occur in almost all sediments studied. It was unambiguously identified by XRD in 4 and some evidence for its occurrence, obtained by FTIR and the Fe:S ratio in oxalate extracts, exists in additional 12 of the 18 sediment samples studied (Table 5). The occurrence of goethite, which was found in 5 of the upper sediment layers, is probably related to the transformation of metastable schwertmannite (cf. below). Similarly, also jarosite, which was identified in 2 of the samples, may be a transformation product. Its origin can be allochthonous in that this mineral is eroded into the lakes from the surrounding dumps, a process assumed to occur in ML 111 (Göttlicher and Gasharova, 2000). In ML 77 and Borna Ost the upper sediment layer as well as the colloidal matter neither contain jarosite nor goethite. This indicates that despite the calculated oversaturation of goethite and jarosite these minerals don't precipitate in these lakes.

The occurrence of schwertmannite in AML is in accordance to the compilation of Bigham and Nordstrom (2000), according to which reddish precipitates found in AMD-influenced waters between pH 2.7 and pH 4 mainly consist of schwertmannite. However, the processes which control the chemical composition of the lake waters, in particular the remarkably constant pH compared to the range of pH values typically found in AMD waters (<0 to 5, e.g., Nordstrom and Alpers, 1994), are not fully understood and will be discussed in the next two sections of this study.

4.2. Processes Regulating the Mineralogy of Iron in AML

4.2.1. Oxidation Kinetics of Fe(II)

Beside the solubility equilibrium between ferric iron, protons and schwertmannite (Fig. 2) the lake water appears also to be at a redox equilibrium. Figure 9 shows a pε-pH diagram for the redox equilibrium between ferrous iron and the ferric iron minerals schwertmannite, jarosite and goethite. The construction of this diagram is based on the equilibria given in Table 2. The K^+ and SO_4^{2-} concentrations were set to the mean value found in the lakes. Into this diagram were plotted the measured pe and pH values of the lake samples. In acidic solutions that contain sufficient concentrations of dissolved Fe(II) and Fe(III) ($>10^{-5}$ M), measured pe values reflect the redox equilibrium between Fe^{2+} and Fe^{3+} (Grundl and Macalady, 1989). Therefore, pe values can be used as a master variable to characterize all equilibria related to these two species. Additionally, Figure 9 contains lines which correspond to the redox equilibrium between Fe^{2+} and the minerals goethite, jarosite and schwertmannite. For the metastable schwertmannite this can be expressed by:

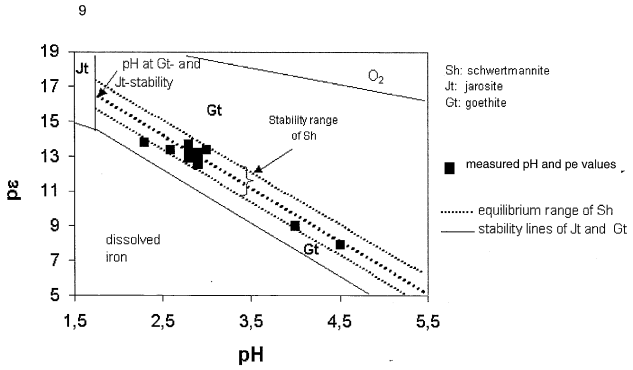

Fig. 9. pε-pH-diagram for the system K-Fe-SO_4. Equilibration lines were calculated using the Eqns. 8 (schwertmannite), 10 (jarosite), and 11 (goethite). the stability line between Jt and Gt was calculated using $KFe_3(SO_4)_2(OH)_6 \leftrightarrow 3\ FeOOH + 3\ H^+ + K^+ + 2\ SO_4^{2-}$ (log K = −13.4) and between H_2O and O_2 using $2\ H_2O \leftrightarrow O_2 + 4\ H^+ + 4\ e^-$ (log K = 86.08). Datapoints represent measured values of pε and pH in the AML.

$$8\ Fe^{2+} + y\ SO_4^{2-} + (24 - 2y + x)/$$
$$2H_2O \rightarrow Fe_8O_8(OH)_x(SO_4)_y + (24 - 2y) \cdot H^+ + 8e^- \quad (7)$$

$$p\varepsilon = \frac{(\log K_{Sh}^* - y\ \log a\ (SO_4^{2-}) - 8 \log a\ (Fe^{2+})}{8 - \frac{24 - 2y}{8pH}} \quad (8)$$

where

$$K_{Sh}^* = (K_{redox}(Fe^{2+}/Fe^{3+}))^8 \cdot IAP_{Sh}, \quad (9)$$

$K_{redox}\ (Fe^{2+}/Fe^{3+}) = 10^{-13}$,

$IAP_{Sh} = 10^{18 \pm 2.5}\ (mol^2 \cdot L^{-2})$, and

$y = 1.5$ (y gives normally a range between 1 and 1.5 mol per mol schwertmannite).

Eqns. 10 and 11 reflect the equilibria between Fe(II) and jarosite and goethite, respectively.

jarosite: pε

$$= \frac{(\log K_{Jt}^* - \log a(K^+) - 2\log a(SO_4^{2-}) - 3\log a(Fe^{2+})}{3 - 2pH} \quad (10)$$

$$\text{goethite: } p\varepsilon = (\log K_{Gt}^* - \log a(Fe^{2+}) - 3pH \quad (11)$$

It appears from Figure 9 that nearly all lake water samples are located in the equilibrium window of the redox couple Fe^{2+}-schwertmannite implying an equilibrium between these two species.

This assumption is confirmed by a mass balance of dissolved Fe(II) and suspended Fe(III) established for the ML 77 (Peine et al., 2000). Solid Fe(III) was identified to be exclusively bound to schwertmannite, of which the sedimentation rate was measured to be $2.6 \cdot 10^{-3}$ M Fe(III) $m^{-2}\ a^{-1}$ on average. The good agreement between this value and the Fe(II) oxidation rate of $3.0 \cdot 10^{-3}$ M Fe(II) $m^{-2}\ a^{-1}$ gives evidence that the rate

at which schwertmannite is formed is controlled by the oxidation kinetics of Fe^{2+}.

Further support for this hypothesis comes from the morphology of schwertmannite particles found in the sediment of ML 77 (Fig. 5). These particles have the same "hedgehog" like structure with long ($\sim$ 200 nm) and thin ($\sim$ 10 nm in diameter) needles as those obtained from the slow schwertmannite synthesis method (method 1, Fig. 5). Such needles were missing in schwertmannite generated with the rapid-synthesis method (method 2, Fig. 5). We assume, that during the fast precipitation crystals hardly grow and the formed crystals of colloidal size agglomerate (stick together) to the observed large spherical particles. Accordingly, the "hedgehog" structure mirrors slow crystal growth. Fe(II) oxidation in acidic waters is slow and can be accelerated through microbial mediation (Stumm and Morgan, 1996). The oxidation rate measured in ML 77 ranges at the lower end of values observed in field studies performed in acidic systems (Kirby et al., 1999) and is only slightly higher than pure chemical oxidation ($1.6 \cdot 10^{-3}$ M a^{-1} at pH 3, c(Fe(II) = 1 mM) and PO_2 = 0.2 atm; rate law from Stumm and Morgan, 1996). The occurrence of Fe(II) oxidizing bacteria in AML has been studied only in the sediments of ML 111, where *Acidithiobacillus ferrooxidans* had been identified at the surface of the sediment of ML 111 with cell numbers between 10^6 and 10^7 per cm^3 (Meier, 2001). It is reasonable to assume microbial oxidation of Fe(II) to take place also in ML 77, which suggests direct interaction between microorganisms and the formation of schwertmannite. Biomineralization of schwertmannite upon oxidation of Fe(II) has been proposed to occur as well in the laboratory by a strain of *Acidithiobacillus ferrooxidans* (Bigham et al., 1990) as in sulfuric acid spring waters (Kawamo and Tomita, 2001). Thus, we suppose the slow crystal growth of schwertmannite is due to the rate-limiting supply of growth nuclei from Fe(II) oxidation in AML.

4.2.2. Complexation and Coordination Chemistry of Iron

In Fe(III) containing solutions, polynuclears of iron(III) oxides and hydroxides form and their structure and that of the crystallizing mineral essentially depend on the pH value and the composition of the solution (Schneider and Schwyn, 1987; Cornell and Schwertmann, 1996). In the AML, chemical speciation of dissolved iron is dominated by sulfate complexes of both Fe(II) and Fe(III) (Table 4). In the following, the effects of these species on the preferential formation of schwertmannite compared to jarosite and goethite in AML are considered.

The high concentration of ferrous iron coordinated with either SO_4^{2-} or HSO_4^- implies that SO_4^{2-} would be already bound to the inner shell of Fe^{2+} during the oxidation process, a ferric sulfate complex being the oxidation product. Thus, OH^- needs to compete with sulfate for coordination sites during the polymerization process, an effect that would eventually inhibit development of a pure (hydr)oxide phase and thus favor schwertmannite formation. From Table 4 it becomes clear that OH^- is still competitive for ferric iron at the pH of the lakes.

These considerations are based on existing knowledge on the formation of akaganéite (β-FeOOH), a mineral whose structure is akin to that of schwertmannite (Bigham et al., 1990) with chloride incorporated into the structure (Murad, 1979) instead of sulfate. It precipitates from acidic $FeCl_3$ solutions (Aktinson, 1977; Music et al., 1982; Schneider, 1984). Therein, as demonstrated by Mössbauer spectroscopy, initially formed polymers of Fe(III) oxide and hydroxide chains already contain some chloride instead of hydroxyl ions (Music et al., 1982). Similar to sulfate, chloride forms complexes with $Fe^{3+}K_{FeCl_2^+} = 10^{1.48}L \cdot mol^{-1}$, which we assume to be precursors for the initial polymerization products. After the formation of oxybridges between these polymers and an incomplete elimination of chlorides in the course of precipitation, the β-FeOOH structure develops wherein chloride is finally electrostatically bound. Analogously, $FeSO_4^+$ could be regarded as a precursor for the postulated bidentate-complex within the structure of schwertmannite (-Fe-O-SO_2-O-Fe-, Bigham et al., 1990). Therefore, we assume that in acidic sulfate solutions, the akaganéite structure will also be the energetically preferred coordination form for ferric iron.

Contrary to the electrostatically bound chloride, sulfate has to share O ions with the Fe(O, $OH)_6$ octaeder by specific interactions (Bigham et al., 1990). This Fe-SO_4 bonding favors polymerization of sulfate due to proper coordination geometry (Hawthorne et al., 2000), but it also leads to the observed distortion of the akaganéite structure in schwertmannite and thus to its weaker crystallinity (Bigham et al., 1990).

The chemical speciation of ferric iron in acidic solutions, however, requires that this statement is only valid at pH values where OH^- ions are competitive with sulfate. Iron(III)-sulfate complexes in solutions appear to prevent the direct formation of goethite at pH $<$ 4. In contrast, below pH 2 a major part of dissolved Fe^{3+} is complexed with sulfate and the formation of an $FeSO_4^+$ complex suppresses the formation of iron(III) hydroxy polymers and subsequent formation of iron(III) oxyhydroxides Music et al. (1982). Jarosite has an average ratio of SO_4: OH of 1: 3, whereas in schwertmannite the ratio of SO_4: OH + O is $\sim$1: 14. These considerations suggest that the pH stability-window of schwertmannite is determined by the chemical speciation of ferric iron. Iron(III) sulfate- and hydroxide complexes appear to prevent the direct formation of the goethite or jarosite structures in that the low-ordered schwertmannite structure is kinetically favored in AML. Ostwald ripening (Cornell and Schwertmann, 1996) will finally lead to transformation into these more stable structures, geochemically predicted according to the supersaturation observed in the AML.

4.2.3. Metastability of Schwertmannite

The redox equilibrium between Fe(II) and schwertmannite observed for most AML (Fig. 9) implies that in these environments schwertmannite is the first mineral formed after Fe(II) oxidation, being metastable with respect to goethite (Bigham et al., 1996) and, at very low pH and in the presence of monovalent cations, also to jarosite. It will therefore tend to transform into one of these minerals within the lake sediments. This process has been demonstrated for goethite in the sediment of ML 77 (Peine et al., 2000). Based on their mineral inventory we assume transformation to occur to goethite in the sediments of at least 4 AML (numbers 2, 11, 12 and 14, Table 5) and to jarosite in those of 2 AML (numbers 3 and 4, Table 5).

From the stability experiments (Figs 6–8) it can be inferred

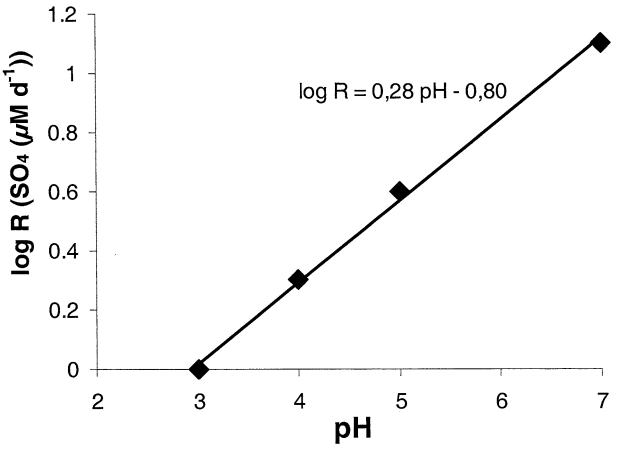

Fig. 10. pH dependence of the initial release rate of sulfate during the first 30 days of the transformation experiments.

that at pH values between 3 and 7 transformation of schwertmannite to goethite takes place. The precipitates at the end of the experiment (after 362 d) consisted, at these pH values, of both minerals in different proportions (Fig. 7). The initial release rate of sulfate follows a zero-order reaction rate and is of fractional order with respect to pH (Fig. 10). This observation is probably due to readsorption of sulfate to the goethite formed, which delineates the slope of the release rate from the theoretical value of $\Delta R_{SO4}/\Delta pH = 1$ derived from the transformation stoichiometry. The constant concentrations of sulfate observed after approx. 30–100 d suggest that internal equilibrium may have already established after this time between the two solid phases, perhaps due to an inhibitory effect of the high sulfate concentrations. Figure 10 clearly demonstrates a pH dependence of the transformation rate with a minimum at pH 3 (1 μM d^{-1}) and increasing rates with increasing pH (12 μM d^{-1} at pH 7). At pH 2, the release of sulfate is accompanied by a high release rate of iron (Fig. 6A). The absence of goethite signals in the IR-spectra and in the X-ray diffractogram (Fig. 7) suggests that proton promoted dissolution of schwertmannite is occurring at this pH. This process may open pathways for the transformation to jarosite. We could not detect jarosite in our experiments due to the absence of Na^+, K^+ or NH_4^+ in the synthesis solutions. However, most of the AML are oversaturated with respect to jarosite (Fig. 2) and jarosite as well as schwertmannite were found in the sediments of ML 107, ML 117 and ML 111 (Tab. 5 and Göttlicher and Gasharova, 2000).

The slow transformation rate observed at pH 3 and 4 helps also to explain the relative stability of schwertmannite found in the upper 3–5 cm of ML 77, corresponding to a sediment age of approx. 2 yr (Peine et al., 2000). Transformation increases upon increase of the pH below this depth from ≈3 to values between 3.5 to 6 by an external proton consuming process, which is the onset of alkalinity generation by sulfate reducing processes (Peine et al., 2000).

4.3. pH Regulation in the AML

The observed pH range for the AML is typical for environments influenced by AMD as observed by Kleeberg (1998) from the study of 25 ML in eastern Germany and by Cravotta et al. (1999) who found that the pH of approx. half of the 793 study sites (Eastern Coal province, USA) ranges between 2.5 and 4.

The pH of the lake waters appears to match stability conditions where neither proton promoted dissolution of schwertmannite nor recrystallization to goethite occur at significant rates at the sediment-water interface (cf. section 4.2.3). This implies that the pH is directly linked to the mineral formation process. We therefore suggest that the pH of AML reflects a steady-state between several processes involved into the formation and consumption of schwertmannite, the mineral being the intermediate product: Preceding to the mineral formation is a steady supply of iron(II) into the lake with seepage waters from the adjacent dumps. These pore waters are anaerobic, weakly acidic and highly concentrated in Fe(II) and sulfate due to iron sulfide oxidation and subsequent weathering reactions in the dumps. Landesumweltamt Brandenburg (1995) surveyed such pore waters in different tailings of two mine sites and found pH values between 4.3 and 7.2, rich in sulfate (15 to 25 mM) and iron (0.7 to 17.1 mM, mainly dissolved and in the ferrous form). Oxygen concentration was either not detectable or at the detection limit. Similar observations were made in sulfide bearing tailings from the exploitation of a sulfide ore body (Germain et al., 1994). Ferrous iron will enter a lake probably as a sulfate complex thereby being oxidized to a ferric sulfate complex $Fe(SO_4)^+$. The subsequent precipitation of schwertmannite is the principle acidifying process. The overall reaction is described by:

$$8\ Fe(SO_4) + 2\ O_2 + (4 + x)\ H_2O \rightarrow Fe_8O_8(OH)_xSO_y + (8 - y)\ SO_4^{2-} + 2\ (8 - y)\ H^+ \quad (12)$$

Peine et al. (2000) determined an acidity production through this process of ≈20 mol m^{-2} a^{-1} in ML 77. To test this hypothesis we performed a scenario according to which a fictitious pore water of a composition described by Landesumweltamt Brandenburg (1995, Table 7) is oxidized to find the pH at which equilibrium exists between the oxidized water and one of the three minerals schwertmannite, jarosite and goethite

Table 7. Composition of the dump pore-water "Meuro" (Landesumweltamt Brandenburg, 1995) and of three fictitious solutions (1, 2, 3) of different Fe(II)-concentrations, which were used to calculate the change of pH upon oxidation of Fe(II) with the modelling program PhreeqC (Fig. 11).

	pH	Fe(II)	SO_4^{2-}	Cl^-	Ca^{2+}	Mg^{2+}	Na^+/K^+
Meuro	6.14	4.6	21.5	2.4	14.8	4.1	1.3
1	6	1	10	–	2	2	1
2	6	5	10	–	2	2	1
3	6	10	10	–	2	2	1

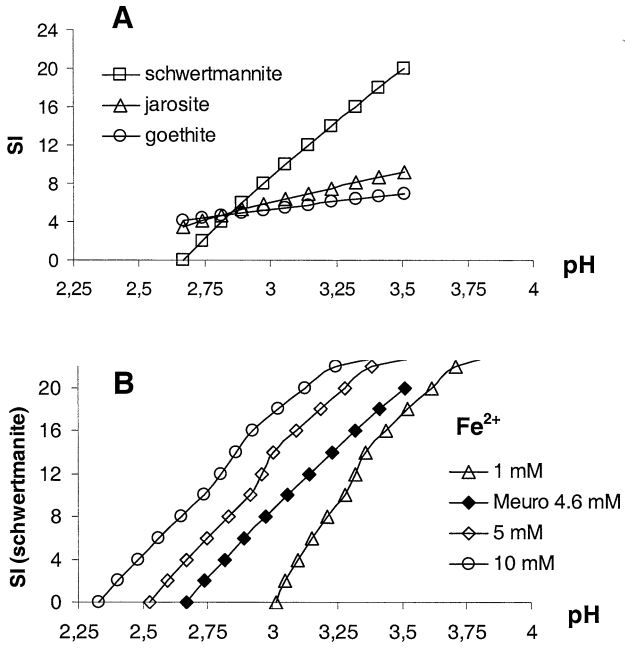

Fig. 11. Change of pH and saturation indices of various iron minerals upon oxidation of Fe(II). Calculations were performed with the geochemical computer code PhreeqC (Nordstrom et al., 1990). Input parameters are given in Table 7. A) Saturation index (SI) of schwertmannite, goethite and jarosite after oxidation of the dump pore-water "Meuro" (Landesumweltamt Brandenburg, 1995). B) Saturation index (SI) of schwertmannite as a function of initial Fe(II)-concentrations.

(sample Meuro in Fig. 11A). At the onset of the oxidation reaction (at high pH), schwertmannite had the highest supersaturation of all three minerals and achieved readily equilibrium with the solution (Fig. 11A). The pH value at which equilibrium is established mainly depends on the initial Fe(II) concentration as demonstrated by the oxidation of three fictitious pore waters with different Fe(II) concentrations (1–10 mM, Table 7). The pH values calculated (2.3 to 3.0; Fig. 11B) satisfactorily match to the pH range measured in the lakes (3.0 $\pm$ 0.6).

Further acidification in the AML upon transformation to goethite (Bigham et al., 1996), seems to be balanced by alkalinity generating processes. Peine et al. (2000) observed that the rate of alkalinity formation from sulfate reduction (2.0 eq m^{-2} a^{-1}) was in the range of the acidity generation due to schwertmannite transformation (3.5 eq m^{-2} a^{-1}) in the sediment of ML 77 and concluded that these two processes balanced each other. We interpret this observation as a coupling of the both reactions, with sulfate reduction being rate limiting for the pH increase and thus driving the transformation reaction.

5. CONCLUSIONS

From this study it becomes obvious that the occurrence of schwertmannite is a common feature of AML, which seem to provide suitable conditions for its formation. These constraints are: (1) the input of pore water of moderate pH containing ferrous iron with sulfate as the predominant anion and (2) oxidation of ferrous iron at low pH, where the rate is slow relative to the precipitation rate of schwertmannite, probably in a biomineralization process. These processes seem to be balanced by the slow transformation to either goethite of jarosite.

The question arises as to whether these observations can be generalized to provide an overall hydrogeochemical model that allows explaining similar observations in other aquatic systems exposed to acid rock drainage. The pathway of iron mineral formation and the pH of the receiving waters will be mainly controlled by the following factors:

- The concentration of ferrous iron, which determines the amount of acidity generated.
- The coordination chemistry of ferric iron: In sulfate-rich waters, competition exists between SO_4^{2-} and OH^- to coordinate with Fe^{3+}, which is reflected by the mineral composition. Accordingly, schwertmannite is the precipitation product at medium acidity.
- The rate of alkalinity supply. Supply of alkalinity is necessary to balance acidification and to control the rate of transformation of schwertmannite to goethite. It is a consequence of microbial mediated sulfate reduction in the AML sediments.
- Hence, aquatic systems, where schwertmannite formation occurs, reflect a stable steady state, balanced by the inflow of potential acidity as $FeSO_4$ with the ground water and by the consumption of acidity within the system.

Acknowledgments—The authors gratefully acknowledge the support from Remo Ender and Joerg Koebcke from the Technical University of Cottbus during sampling and from Clarissa Drummer (University of Bayreuth) for preparing the SEM-photos. The Deutsche Forschungsgemeinschaft (DFG) provided financial support. This study was part of the priority program 546 "Geochemical processes with long-term effects in anthropogenically affected seepage and groundwater" (Pe 438/5-1).

Associate editor: C. M. Eggleston

REFERENCES

Aktinson R. J. (1977) Crystal nucleation and growth in hydrolysing iron(III)chloride solutions. *Clays Clay Minerals* **25,** 49–56.

Bigham J. M., Schwertmann U., Carlson L., and Murad E. (1990) A poorly crystallized oxyhydoxysulfate of iron formed by bacterial oxidation of Fe(II) in acid mine waters. *Geochim. Cosmochim. Acta* **54,** 2743–2758.

Bigham J. M., Carlson L., and Murad E. (1994) Schwertmannite a new iron oxyhydroxysulfate from Pyhäsalmi, Finland, and other localities. *Min. Mag.* **58** *(393),* 641–648.

Bigham J. M., Schwertmann U., Traina S. J., Winland R. L., and Wolf M. (1996) Schwertmannite and the chemical modeling of iron in acid sulfate waters. *Geochim. Cosmochim. Acta* **60,** 2111–2121.

Bigham J. M. and Nordstrom D. K. (2000) Iron and aluminium hydroxysulfates from acid sulfate waters. In *Reviews in Mineralogy and Geochemistry* (eds. C. N. Alpers, J. L. Jambor, and D. K. Nordstrom), pp. 351–403. Mineralogical Society of America.

Carlson L. and Schwertmann U. (1981) Natural ferrihydrites in surface deposits from Finland and their association with silica. *Geochim. Cosmochim. Acta* **45,** 421–429.

Childs C. W., Inoe K., Mizota C., Soma M. and Theng B. K. G. (1998) Natural schwertmannite formed in a lake from waters draining pyrite deposits. In *Water-Rock Interaction* (eds. G. B. Arehart and J. R. Hulston), pp. 923–926. Balkema, Rotterdam.

Cornell R. and M.Schwertmann U. (1996) *The Iron Oxides.* VCH.

Cravotta C. A. I., Brady K. B. C., Rose A. W., and Douds J. B. (1999) Frequency distribution of the pH of coal-mine drainage in Pennsylvania DW. In *U.S. Geological Survey Toxic Substances Hydrology*

Program-Proc. Technical Meeting (ed. D. W. Morganwalp), pp. 313–324. Report 99-4018A. U.S. Geological Survey, Water-Resources Investigation.

Farmer V. C. (1974) The Infrared Spectra of Minerals. Minerological Society, London.

Geller W., Klapper H., and Schultze M. (1998) Natural and anthropogenic sulfuric acidification of lakes. In *Acidic Mining Lakes* Geller W., Klapper H., and Salomons W., pp. 3–14. Springer.

Germain M. D., Tassé N., and Bergeron M. (1994) Limit to self-neutralization in acid mine tailings: The case of East-Sullivan, Québec, Canada. In *Environmental Geochemistry of Sulfide Oxidation* (eds. D. W. Blowes and C. N. Alpers), pp. 365–379. Symposium Series 550, American Chemical Society.

Göttlicher J., and Gasharova B. (2000) Interactions of iron and sulfur bearing solid phases with water in surface coal mining pits and acidic mining lakes. In *Applied Mineralogy* (eds Rammlmayr et al.), p. 1048. Balkema.

Grundl T. and Macalady D. (1989) Electrode measurements of redox potential in anaerobic ferric ferrous chloride systems. *J. Cont. Hydrol.* **5,** 97–117.

Hawthorne F. C., Krivovichev S. V. and Burns P. C. (2000) The crystal chemistry of sulfate minerals. In *Sulfate Minerals*, Vol. 40 (eds. C. N. Alpers, J. L. Jambor and D. K. Nordstrom), p. 608. Mineralogical Society of America.

Kawano M. and Tomita K. (2001) Geochemical modeling of bacterially induced mineralization of schwertmannite and jarosite in sulfuric acid spring water. *Am. Mineral.* **86,** 1156–1165.

Kirby C. S., Thomas H. M., Southam G., and Donald R. (1999) Relative contributions of abiotic and biological factors in Fe(II) oxidation in mine drainage. *Appl. Geochem.* **14,** 511–530.

Kleeberg A. (1998) The quantification of sulfate reduction in sulfate-rich freshwater lakes—A means for predicting the eutrophication process of acidic mining lakes? *Water Air Soil Pollut.* **108,** 365–374.

Krüger G., Erzinger J., and Kaufmann H. (1998) Laboratory and airborne reflectance spectrometric analyses of lignite overburden dumps. *J. Geochem. Explor.* **64,** 47–65.

Küsel K., Dorsch T., Acker G., and Stackebrandt E. (1999) Microbial reduction of Fe(III) in acidic sediments: Isolation of Acidiphilium cryptum JF-5 capable of coupling the reduction of Fe(III) to the oxidation of glucose. *Appl. Environ. Microbiol.* **65,** 3633–3640.

Landesumweltamt Brandenburg. (1995) Wasserbeschaffenheit in Tagebaurestseen. In *Studien und Tagungsberichte*, Vol. 6 (ed. Landesumweltamt Brandenburg), 86 p. Potsdam.

LMBV. (1997) Gutachten zur Entwicklung der Wasserbeschaffenheit in den Tagebaurestseen. Senftenberg/Cottbus.

Meier J. (2001) Untersuchungen zum mikrobiellen Schwefelkreislauf in sauren Tagebau-Restseen der Niederlausitz (Brandenburg). Ph.D. thesis. Universität Bonn.

Meyer R. K. F. and Mielke H. (1993) Geologische Karte von Bayern 1: 25 000. In *Erläuterungen zu Blatt* Nr. 6639, *Wackersdorf* (eds. R. K. F. Meyer and H. Mielke), pp. 153–164. Bayerisches Geologisches Landesamt.

Meyer R. K. F. and Poschlod K. (1993) Tertiäre Braunkohle. In Meyer R. K. F. and Mielke H. (1993) Geologische Karte von Bayern 1: 25 000, *Erläuterungen zu Blatt*Nr. 6639, *Wackersdorf* (eds. R. K. F. Meyer and K. Poschlod), pp. 153–164. Bayerisches Geologisches Landesamt.

Murad E. (1979) Mössbauer and X-ray data on FeOOH (akaganéite). *Clay Minerals* **14,** 273–283.

Music S., Vertes A., Simmons G. W., Dzako-Nagy I., and Leidheiser H., Jr. (1982) Mössbauer spectroscopic study of the formation of Fe(III) oxyhydroxides and oxides by hydrolysis of aqueous Fe(III) salt solutions. *J. Colloid Interface Sci.* **85,** 256–265.

Nordstrom D. K., Plummer L. N., Langmuir D., Busenberg E., May H. M., Jones B. E., and Parkhurst D. L. (1990) Revised chemical equilibrium data for major water-mineral reactions and their limitations. In *Chemical Modeling of Aqueous Systems 2* (eds. D. L. Melchior and R. L. Bassett), pp. 398–413. Symposium Series 416, ACS.

Nordstrom D. K. and Alpers C. N. (1994) Geochemistry of acid mine water. In *The Environmental Geochemistry of Mineral Deposits* (eds. Plumlee G. S. and Logsdon M. K.), pp. 133–160. Reviews in Economic Geology. Society of Economic Geologists.

Nowel W., Bönisch R., Schneider W., and Schulze H. (1995) *Geologie des Lausitzer Braunkohlereviers*. Lausitzer Braunkohle.

Parkhurst D. L. (1995) *User's Guide to PHREEQC: A Computer Program for Speciation, Reaction-Path, Advective Transport and Inverse Geochemical Calculations*. Report, Water Resources Division. Geological Survey.

Parkhurst D. L. and Appelo C. A. J. (1999) *User's Guide to PHREEQC—A Computer Program for Speciation, Reaction Path, 1d-Transport and Inverse Geochemical Calculation*. Report 99-4259. U.S. Geological Survey. Water-Resources Investigations.

Peine A. (1998) Saure Restseen des Braunkohletagebaus—Charakterisierung und Quantifizierung biogeochemischer Prozesse und Abschätzung ihrer Bedeutung für die seeinterne Neutralisierung. Ph.D. thesis. University of Bayreuth, Germany.

Peine A., Trischler A., Küsel K., and Peiffer S. (2000) Electron flow in an iron-rich acidic sediment—Evidence for an acidity-driven iron cycle. *Limnol. Oceanogr.* **45,** 1077–1087.

Schneider W. (1984) Hydrolysis of iron(III)-chaotic olation versus nucleation. *Comments Inorg. Chem.* **3,** 205–223.

Schneider W. and Schwyn B. (1987) The hydrolysis of iron in synthetic, biological and aquatic media. In *Aquatic Surface Chemistry* (ed. W. Stumm), pp. 167–196. Wiley Interscience.

Schwertmann U., Bigham J. M., and Murad E. (1995) The first occurrence of schwertmannite in a natural stream environment. *Eur. J. Min.* **7,** 547–552.

Stumm W. and Morgan J. J. (1996) *Aquatic Chemistry—Chemical Equilibrium and Rates in Natural Waters*. 3rd ed. Wiley.

Tamura H., Goto K., Yotsuyanagi T., and Nagayam M. (1974) Spectrophotometric determination of iron(II) with 1,10-Phenantroline in the presence of large amounts of iron (III). *Talanta* **21,** 314–318.

Van der Marel H. W. and Beutelspacher H. (1976) *Atlas of Infrared Spectroscopy of Clay Minerals and Their Admixtures*. Elsevier.

Yu J. Y., Heo B., Choi I. K., Cho J. P., and Chang H. W. (1999) Apparent solubilities of schwertmannite and ferrihydrite in natural stream water polluted by mine drainage. *Geochim. Cosmochim. Acta* **63,** 3407–3416.